Modeling for Energy Consumption Evaluation

Mission profiles, powertrain characteristics, and vehicle specifications, are fundamental to the evaluation of the energy consumption of a vehicle propulsion system. In this chapter, powertrain components of various vehicle propulsion systems are analytically modeled at descriptive and predictive level. Specifically, descriptive analytic models estimate the intrinsic features; whereas predictive analytic models predict those features for components of different dimensioning parameters. In addition, vehicle load is analytically estimated for the evaluation of energy consumption over a mission.

2.1 Modeling of Vehicle Propulsion System

Vehicle propulsion systems of conventional, battery-electric, and hybrid-electric vehicles are significantly different from each other due to the composition of powertrain components and control system. The main powertrain components are composed of Internal Combustion Engine (ENG), Transmission (TRA), Battery (BAT), and Electric Motor/Generator (EMG), as depicted in Fig. 2.1.

The main powertrain components are analytically modeled to estimate the energy consumption of a vehicle over a specified mission in an accurate and rapid way. The analytic models are control-oriented to develop optimal control techniques for hybrid-electric vehicles. Moreover, these analytic models are design-oriented as well for the optimization of dimensioning parameters. In other words, they are scalable. As a consequence, the analytic models of powertrain components are established at two

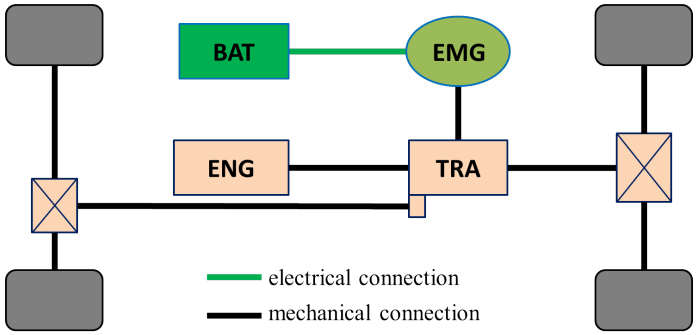

Figure 2.1 – Main powertrain components of a parallel hybrid-electric vehicle.

distinct levels: the descriptive and predictive level.

At descriptive level, ***descriptive analytic models*** describe the main features of a specific powertrain component, such as the energy losses of an ENG. The descriptive analytic model is directly applied for the energy consumption evaluation of any given vehicles, and for the optimal control laws identification for hybrid-electric vehicles. Parameters of descriptive analytic models are identified from each powertrain component.

At predictive level, ***predictive analytic models***, on the other hand, allow the prediction of the main features for powertrain components of different dimensioning parameters. For instance, the power losses of an ENG of the varied engine displacements can be approximated by predictive analytic models. Coefficients in predictive analytic models are identified from the identification set of powertrain components in the same family of technology.

To validate descriptive and predictive analytic models, estimations are compared with grid-point data. For the sake of clarity, the results estimated by descriptive analytic models alone are designated as **description** in the following sections; whereas, results approximated by predictive analytic models are designated as **prediction**.

To present the accuracy of descriptive and predictive analytic models, the mean relative error between description and grid point data is denoted by ε^d; whereas, the relative mean error between description and grid-point data is indicated by ε^p. Regardless of descriptive or predictive error, the mean relative error, denoted by subscript c, is evaluated for each powertrain component in its identification set. In contrast, the average relative error is evaluated based on the whole identification set, and indicated by the subscript s. Statistic characteristics between estimations (description and prediction) and grid-point data are illustrated to supplement the mean relative error of each component.

Apart from the validation at powertrain component and identification set level,

the accuracy of descriptive and predictive analytic models is investigated at vehicle propulsion system level. At the propulsion system level, the energy consumption is estimated based on different types of powertrain data for various types of vehicle propulsion systems. The powertrain data consists of grid-point data, description, and prediction; whereas vehicle propulsion systems include conventional, battery-electric, and hybrid-electric vehicles. The accuracy of analytic models is most important at vehicle propulsion system level since it determines their validity. The difference of energy consumption of different vehicle propulsion systems will be demonstrated in Chapter 3.3 and 4.5.

Considering the perspective of system identification, the proposed analytic models are needed to validate with components different from the identification set, particularly the predictive analytic models. However, analytic models of powertrain components are validated from the corresponding identification sets due to the availability of data.

2.2 Internal Combustion Engine

As the primary power source in a conventional or hybrid-electric vehicle, an internal combustion engine (ENG) provides mechanical power to propel the vehicle by burning hydrocarbon-containing fuels, such as gasoline, diesel, natural gas, and bio-fuels. The ENGs can be classified with respect to various criteria. Concerning the ignition method, there are Spark Ignition (SI) and Compression Ignition (CI) engines. Regarding the charging technology, it is composed of Naturally Aspirated (NA) and Turbo-Charged (TC) method. In regard to NA engines, engineers develop various combustion modes, such as Stoichiometric-Burn (SB) and Lean-Burn (LB) methods.

2.2.1 Dimensioning Parameter

The technological dimensioning parameter of ENGs, denoted by $\mathcal{I}_e$, contains four types of engines for light-duty vehicles, which are combinations of different engine technologies. Four types of engines are listed in $\mathcal{I}_e = \{\text{SI/NA/SB}, \text{SI/NA/LB}, \text{SI/TC}, \text{CI/TC}\}$, and represented by integers in the design optimization of vehicle propulsion systems.

Apart from the technological parameter $\mathcal{I}_e$, dimensioning parameters of an engine are essential to develop predictive analytic models. The overall dimensioning parameter set is defined as

$$\mathcal{S}_e = \{\mathcal{I}_e, \mathcal{V}_e, \mathcal{T}_e, \mathcal{P}_e, \mathcal{N}_{eT}, \mathcal{N}_{eP}\}, \tag{2.1}$$

where $\mathcal{V}_e$ is engine displacement in [m^3], $\mathcal{T}_e$ is the rated engine torque in [Nm], $\mathcal{P}_e$ is the rated engine power in [kW], $\mathcal{N}_{eT}$ and $\mathcal{N}_{eP}$ are engine speeds in [rpm] corresponding to the rated torque and the rated power.

Although engine displacement, rated torque, and rated power are listed separately, they are not independent from each other. The rated torque and rated power depend on engine displacement because of the similar maximum brake mean effective pressure.

2.2.2 Analytic Model

Parameterization of the engine fuel consumption map is performed for both light- and heavy-duty engines. Accordingly, analytic models at both descriptive and predictive level are developed and validated separately.

At Descriptive Level

Inspired by the Willans line models [63], the descriptive analytic models of internal combustion engines evaluate the burned fuel power as a function of engine speed and engine brake power. The burned fuel power is converted directly from fuel consumption maps by taking the lower heating value of fuel into account. The chosen descriptive analytic model for light-duty engines is expressed by

$$P_{ef}(\omega_e, P_e) = \begin{cases} k_{e0}(\omega_e) + k_{e1}(\omega_e) P_e, & P_e \leq P_{ec}(\omega_e) \\ k_{e0}(\omega_e) + (k_{e1}(\omega_e) - k_{e2})\, P_{ec}(\omega_e) + k_{e2} P_e, & P_e > P_{ec}(\omega_e) \end{cases}, \tag{2.2}$$

where ω_e is the engine speed in [rad/s]; P_e is the engine brake power of engine in [W]; P_{ec} is the engine corner power of maximal efficiency [W], whose corresponding torque is depicted in Fig. 2.2; and P_{ef} is the power of burned fuel in [W], which is converted from the mass flow rate of an engine map. Parameters $k_{ei}(i = 0, 1, 2)$ are identified for each individual engine from the engine identification set of Table 2.4.

Concerning turbo-charged diesel engines for heavy-duty applications, the descriptive analytic model is

$$P_{ef}(\omega_e, P_e) = k_{e3}(\omega_e) + k_{e4}(\omega_e) P_e + k_{e5}(\omega_e) P_e^2, \tag{2.3}$$

where parameters $k_{ei}(i = 3, 4, 5)$ are identified for each individual engine in its identification set of Table 2.5.

In addition to analytic models of burned fuel power, the full-load torque of an ENG is modeled analytically as well. Concerning SI/NA ENGs for light-duty applications,

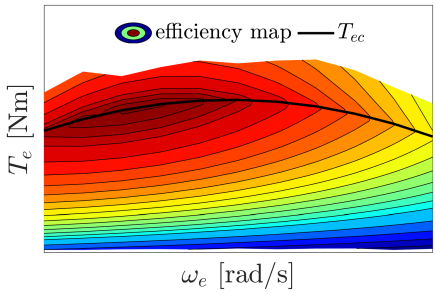

Figure 2.2 – Corner torque T_{ec} of an internal combustion engine.

the analytic model of full-load torque is

$$\overline{T}_e(\omega_e) = k_{e6} + k_{e7}\omega_e + k_{e8}\omega_e^2, \tag{2.4}$$

where $\overline{T}_e$ is the full-load torque. As a convention, variables with over-line (e.g. $\overline{T}$) indicates the maximum admissible value; whereas, the under-line (e.g. $\underline{T}$) represents the minimum admissible value.

Parameters $k_{ei}(i = 6, 7, 8)$ are identified by solving the following linear system that contains the engine dimensioning parameters $\mathcal{T}_e$, $\mathcal{P}_e$, $\mathcal{N}_{eT}$, and $\mathcal{N}_{eP}$.

$$\begin{bmatrix} 1 & \frac{1000\pi}{30} & \left(\frac{1000\pi}{30}\right)^2 \\ 1 & \frac{\mathcal{N}_{eT}\pi}{30} & \left(\frac{\mathcal{N}_{eT}\pi}{30}\right)^2 \\ 1 & \frac{\mathcal{N}_{eP}\pi}{30} & \left(\frac{\mathcal{N}_{eT}\pi}{30}\right)^2 \end{bmatrix} \begin{bmatrix} k_{e6} \\ k_{e7} \\ k_{e8} \end{bmatrix} = \begin{bmatrix} T_{ek} \\ \mathcal{T}_e \\ \frac{30\mathcal{P}_e}{\pi\mathcal{N}_{eP}} \end{bmatrix}, \tag{2.5}$$

where T_{ek} is the engine torque at 1000 rpm for light-duty engines.

Regardless of light-duty or heavy-duty engines, turbocharged engines have a piecewise analytic model to approximate the full-load torque,

$$\overline{T}_e(\omega_e) = \begin{cases} k_{e9} + k_{e10}\omega_e, & w_e \le \frac{\pi\mathcal{N}_{eT1}}{30} \\ \mathcal{T}_e, & \frac{\pi\mathcal{N}_{eT1}}{30} \le w_e \le \frac{\pi\mathcal{N}_{eT2}}{30} \\ k_{e11} + k_{e12}\omega_e, & w_e \ge \frac{\pi\mathcal{N}_{eT2}}{30} \end{cases}, \tag{2.6}$$

where $\mathcal{N}_{eT1}$ and $\mathcal{N}_{eT2}$ are the minimal and maximal speed of the rated torque, respectively.

Parameters k_{e9} and k_{e10}, k_{e11} and k_{e12} are identified by solving the following two linear equation systems,

$$\begin{bmatrix} 1 & \frac{1000\pi}{30} \\ 1 & \frac{\pi \mathcal{N}_{eT1}}{30} \end{bmatrix} \begin{bmatrix} k_{e9} \\ k_{e10} \end{bmatrix} = \begin{bmatrix} T_{ek} \\ \mathcal{T}_e \end{bmatrix}, \tag{2.7}$$

and

$$\begin{bmatrix} 1 & \frac{\pi \mathcal{N}_{eT2}}{30} \\ 1 & \frac{\pi \mathcal{N}_{eP}}{30} \end{bmatrix} \begin{bmatrix} k_{e11} \\ k_{e12} \end{bmatrix} = \begin{bmatrix} \mathcal{T}_e \\ \frac{30\mathcal{P}_e}{\pi \mathcal{N}_{eP}} \end{bmatrix}, \tag{2.8}$$

where engine speed $\mathcal{N}_{eT1}$, $\mathcal{N}_{eT2}$, and $\mathcal{N}_{eP}$ are indicated in Fig. 2.3.

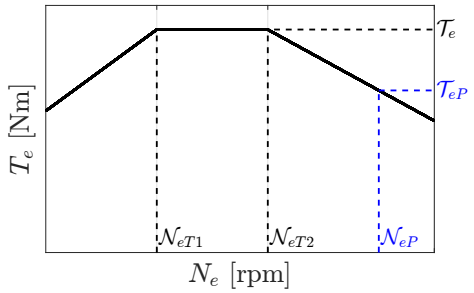

Figure 2.3 – Speed variables of turbocharged internal combustion engines.

At Predictive Level

Parameters $k_{ei}(i = 0, \cdots, 12)$ in descriptive analytic models in Eq. 2.2 and 2.3 are further expressed as function of engine dimensioning parameters. As for light-duty engines, their predictive analytic models are expressed by

$$k_{e0} = \frac{\mathcal{V}_e \omega_e}{4\pi} \left(c_{e1} + \frac{30 c_{e2} \omega_e}{\pi} \right), \tag{2.9}$$

$$k_{e1} = c_{e3} + \frac{30 c_{e4} \omega_e}{\pi} + \frac{900 c_{e5} \omega_e^2}{\pi^2}, \tag{2.10}$$

$$k_{e2} = c_{e6}, \tag{2.11}$$

where coefficients $c_{ei}(i = 1, \cdots, 6)$, depending on engine-technological parameter $\mathcal{I}_e$, are listed in Table 2.1.

$\mathcal{I}_e$	c_{e1}	c_{e2}	c_{e3}	c_{e4}	c_{e5}	c_{e6}
SI/LB	3.24×10^5	54.0	2.541	-1.892 $\times10^{-4}$	3.863 $\times10^{-8}$	4.546
SI/SB			2.456	-4.349 $\times10^{-5}$	1.032 $\times10^{-8}$	
CI	1.84×10^5	112.5	2.363	0	0	3.061

Table 2.1 – Values of coefficients $c_{ei}(i=1,\cdots,6)$ for light-duty engines.

The engine corner power in the piece-wise linear model of burned fuel power in Eq. 2.2 is calculated by

$$P_{ec}(\omega_e)=\begin{cases}0.8\omega_e\overline{T}_e(\omega_e), & NA,\\ \dfrac{1000\mathcal{V}_e\omega_e}{4\pi}\sum_{i=7}^{14}c_{ei}\left(\dfrac{\omega_e}{2\pi}\right)^{i-7}, & TC,\end{cases} \tag{2.12}$$

where coefficients $c_{ei}(i=7,\cdots,14)$ are taken from the PERE Report [64]. Their values are presented in Table 2.2 correspondingly for spark ignition (SI) and compression ignition (CI) engines.

$\mathcal{I}_e$	c_{e7}	c_{e8}	c_{e9}	c_{e10}
SI	-1200.5	298.93	-17.586	0.56342
CI	-19950.8	3479.90	-231.809	8.25775
$\mathcal{I}_e$	c_{e11}	c_{e12}	c_{e13}	c_{e14}
SI	-0.010463	1.132 $\times10^{-4}$	-6.645 $\times10^{-7}$	1.631 $\times10^{-9}$
CI	-0.169919	2.023 $\times10^{-3}$	-1.292 $\times10^{-5}$	3.422 $\times10^{-8}$

Table 2.2 – Values of coefficients $c_{ei}(i=7,\cdots,14)$ for light-duty engines.

At the predictive level, the torque at 1000 rpm for light-duty engines is estimated by

$$T_{ek}=\begin{cases}\dfrac{1000\mathcal{V}_e}{4\pi}\sum_{i=7}^{14}c_{ei}\left(\dfrac{\omega_e}{2\pi}\right)^{i-7}, & NA,\\ \dfrac{11\times10^8\mathcal{V}_e}{4\pi}, & TC.\end{cases} \tag{2.13}$$

Concerning heavy-duty engines, their predictive analytic models are written as follows:

$$k_{e3}=\frac{10^5\mathcal{V}_e\omega_e}{4\pi}\left(c_{e15}+c_{e16}\omega_e+c_{e17}\omega_e^2\right), \tag{2.14}$$

$$k_{e4}=10^5c_{e18}, \tag{2.15}$$

$$k_{e5}=\frac{4\times10^5\pi}{\mathcal{V}_e\omega_e}\left(c_{e19}+c_{e20}\omega_e+c_{e21}\omega_e^2\right), \tag{2.16}$$

where coefficients $c_{ei}(i = 15, \cdots, 21)$ are listed in Table 2.3.

c_{e15}	c_{e16}	c_{e17}	c_{e18}	c_{e19}	c_{e20}	c_{e21}
2.000	2.190×10^{-3}	7.008×10^{-5}	1.884	8.549×10^{-2}	1.024×10^{-3}	3.435×10^{-6}

Table 2.3 – Values of coefficients $c_{ei}(i = 15, \cdots, 21)$ for heavy-duty engines.

2.2.3 Model Validation

The identification sets of engines are introduced in terms of light- and heavy-duty applications, respectively. The whole identification set is implemented to develop descriptive and predictive analytic models, and to validate these models. After the demonstration of engine grid-point data in terms of maps, the mean relative error and statistic characteristics are illustrated and discussed hereafter.

Identification Set

Due to different vehicle applications, two types of engine identification sets are used to develop and validate the descriptive and predictive analytic models. The identification set of light-duty engines is listed in Table 2.4, including specifications of the dimensioning parameters; whereas the set of heavy-duty engines is summarized in Table 2.5, containing corresponding specifications of the dimensioning parameters.

ID	$\mathcal{I}_e$	$\mathcal{V}_e$ [L]	$\mathcal{T}_e$ [Nm]	$\mathcal{N}_{eT}$ [rpm]	$\mathcal{P}_e$ [kW]	$\mathcal{N}_{eP}$ [rpm]
1	CI/TC	2.2	292	2000	90	4000
2	CI/TC	1.6	242	1750	80	4000
3	CI/TC	2.0	324	2000	98	4000
4	CI/TC	2.2	327	1750	88	3000
5	CI/TC	1.5	202	2000	78	4000
6	CI/TC	2.0	368	1750	121	4000
7	CI/TC	1.2	145	2000	43	4000
8	SI/TC	0.9	145	3000	58	5000
9	SI/NA/LB	1.5	120	4500	60	5500
10	SI/NA/LB	1.9	166	4000	82	5000
11	SI/TC	2.0	302	2500	150	5000
12	SI/TC	1.8	312	2000	148	5500
13	SI/NA/SB	1.0	95	4000	54	6000
14	SI/NA/LB	1.4	128	4500	70	5500

Table 2.4 – Identification set of light-duty engines.

ID	$\mathcal{I}_e$	$\mathcal{V}_e$ [L]	$\mathcal{T}_e$ [Nm]	$\mathcal{N}_{eT}$ [rpm]	$\mathcal{P}_e$ [kW]	$\mathcal{N}_{eP}$ [rpm]
1	CI/TC	9.3	1600	1050	235	1900
2	CI/TC	9.3	1400	1000	210	1700
3	CI/TC	12.7	2375	1000	335	1700
4	CI/TC	12.7	2375	1000	340	1700
5	CI/TC	12.7	2350	1000	358	1600
6	CI/TC	12.7	2275	1000	325	1700
7	CI/TC	12.7	2600	1000	376	1700
8	CI/TC	16.4	3000	1000	444	1700
9	CI/TC	16.4	3000	1000	490	1700
10	CI/TC	16.4	3500	1000	544	1900

Table 2.5 – Identification set of heavy-duty engines.

Result

Description and prediction of each engine are comparatively illustrated with respect to the grid-point data. For simplicity reason, one light- and one heavy-duty engine are exemplified individually. The comparisons among grid-point data, description, and prediction of other engines are found in Appendix B.1.

Fig. 2.4 demonstrates the grid-point data, description, and prediction in terms of burned fuel power for ENG ID1. As shown in Fig. 2.4c, the contour lines of prediction are smoothest compared with the grid-point data and the description. Nonetheless, both description and prediction present a similar trend compared with the grid-point data.

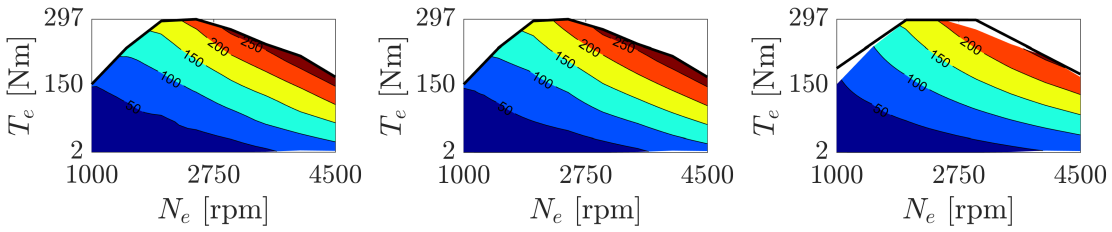

(a) grid-point data (b) description (c) prediction

Figure 2.4 – Map of burned fuel power of light-duty engine ID1.

Concerning the exemplified heavy-duty engine, the grid-point data, description, and prediction of ENG ID2 are comparatively depicted in terms of efficiency in Fig. 2.5. Due to confidential issues, the horizontal and vertical axis are scaled compared to original data. The best efficiency area of prediction are enlarged significantly, as illustrated in

Fig. 2.5c. Nevertheless, the description and prediction are still comparable with respect to the grid-point data.

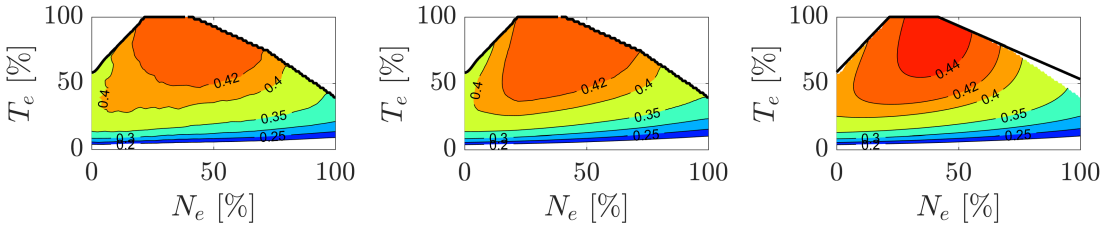

(a) grid-point data (b) description (c) prediction

Figure 2.5 – Efficiency map of heavy-duty engine ID2.

Analysis

The analysis of mean relative error and linear regression is performed to evaluate the accuracy of descriptive and predictive analytic models for both light- and heavy-duty engines. In particular, analysis of mean relative error is completed both for each engine and the whole engine identifications set. Then, the exemplified light- and heavy-duty engine are used to depict their contour maps of mean relative error and the linear regression analysis.

Mean relative errors – including the mean description error of each component ε_c^d, the mean prediction error of each component ε_c^p, the average description error of whole identification set ε_s^d, and the average prediction error of whole identification set ε_s^p – are illustrated in Fig. 2.6 for both light- and heavy-duty engines. In summary, the maximum of mean relative error was 7.7% for light-duty engine ID10. The mean relative error of heavy-duty engine identification set is lower than that of light-duty engine identification set.

Considering light-duty engine ID1, its descriptive and predictive relative errors are illustrated in Fig. 2.7a and Fig. 2.7b, respectively. Clearly, large errors occur at the high engine speed and high load zone particularly for predictive analytic models.

Linear regression analysis is separately carried out between the description and the grid-point data, and between the prediction and the grid-point data. The power of burned fuel is normalized to a constant value. Fig. 2.8 presents the corresponding characteristics. To summarize, the descriptive analytic models can well represent grid-point data. Albeit the predictive analytic models have a smaller value of r^2, it can still predict the grid-point data for the intended study of vehicle energy consumption.

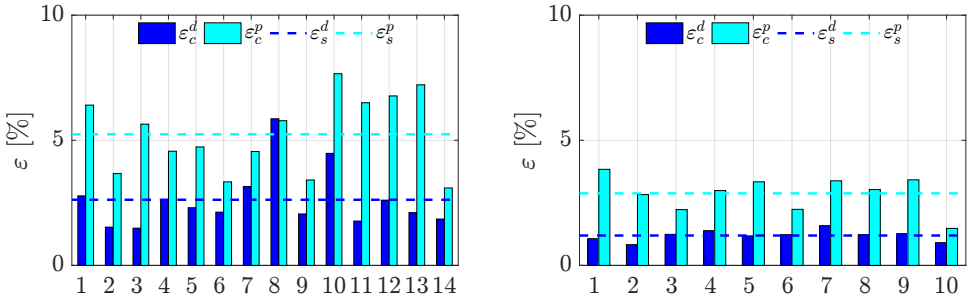

(a) light-duty engines (b) heavy-duty engines

Figure 2.6 – Mean relative error of each engine and the whole identification set.

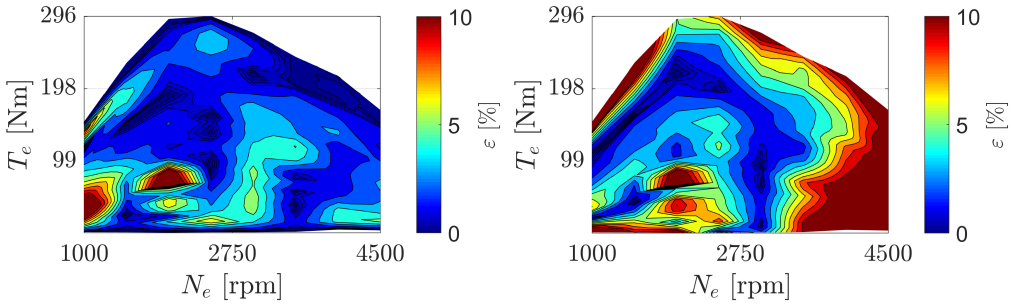

(a) descriptive error map (b) predictive error map

Figure 2.7 – Maps of relative errors of light-duty engine ID1.

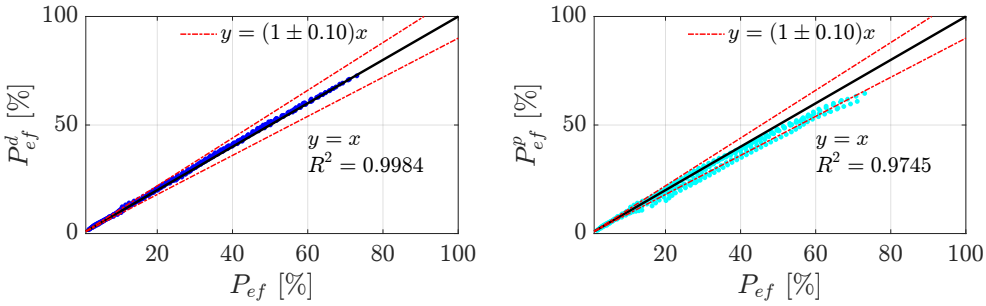

(a) between description and data (b) between prediction and data

Figure 2.8 – Comparison of burned fuel power for light-duty engine ID1.

As for the heavy-duty engine ID2, the descriptive and predictive maps of mean relative errors are depicted in Fig. 2.9. The mean relative errors of both level analytic models are at low level. In details, high errors only occur in extremely low load condition

for the descriptive analytic models; whereas high errors are shifted to slightly higher-load and lower-speed zone for the predictive analytic models.

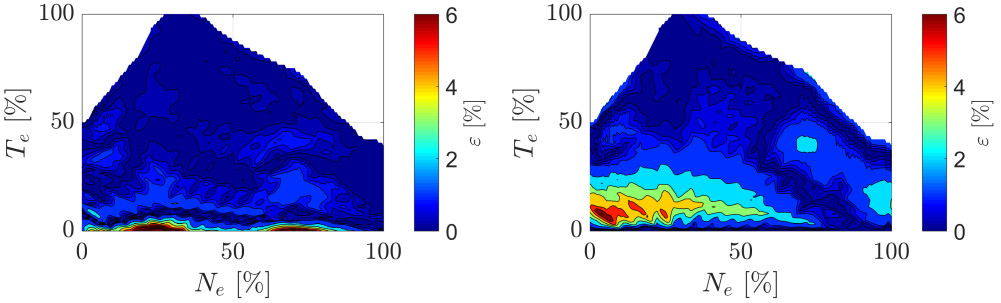

(a) descriptive error map (b) predictive error map

Figure 2.9 – Maps of relative errors of heavy-duty engine ID2.

Linear regression analysis is carried out for the heavy-duty engine ID2 in a similar way as for light-duty engine ID1. Results are correspondingly summarized in Fig. 2.10, where values of r^2 are presented. The high r^2 values indicate the goodness of developed analytic models.

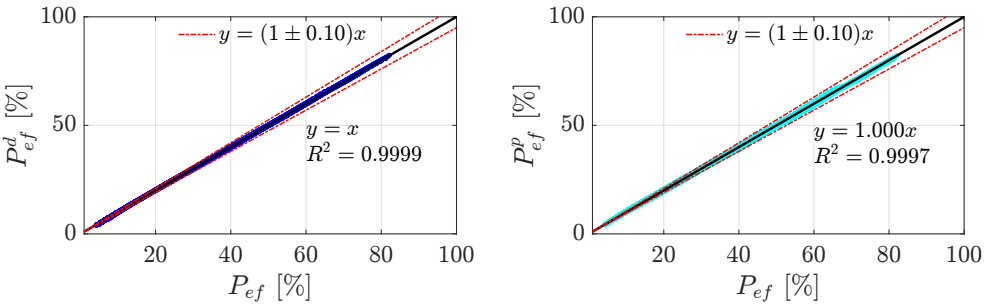

(a) between description and data (b) between prediction and data

Figure 2.10 – Comparison of burned fuel power for heavy-duty engine ID2.

2.3 Drivetrain

Drivetrain delivers power from engine or electric motor to drive wheels. The main components of a drivetrain consist of a transmission, a final drive, and other simple gear-trains, depending on their technologies. Compared with the universal configuration in [65], Fig. 2.11 depicts an updated version for various vehicle propulsion systems,

including conventional, battery-electric, and hybrid-electric vehicle. Ratios of transmission and final drive are denoted by $\mathcal{R}_t$ and $\mathcal{R}_{fd}$, respectively; whereas parameter $\mathcal{R}_e$ and $\mathcal{R}_g$ denote the ratio between engine shaft and node N_1, and the ratio gear between electric generator shaft and note N_1, respectively. In addition, parameter $\mathcal{R}_m$ means the ratio between electric motor shaft and node N_2.

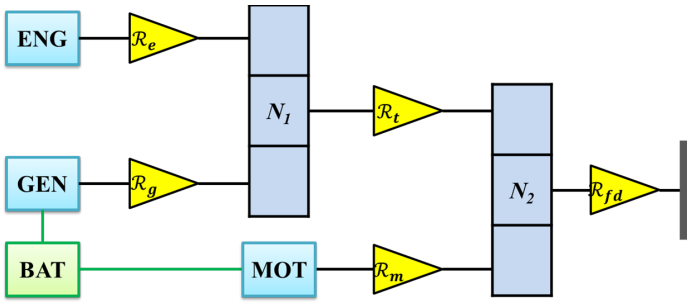

Figure 2.11 – Universal configuration of vehicle propulsion systems.

In a conventional vehicle, the drivetrain consists of transmission $\mathcal{R}_t$ and final drive $\mathcal{R}_{fd}$; in a battery-electric vehicle, the drivetrain is composed of simple gear-train $\mathcal{R}_m$ and final drive $\mathcal{R}_{fd}$; in a hybrid-electric vehicle, components of drivetrain depend on the powertrain architecture. For example, the drivetrain of a series HEV may consist of gear-train $\mathcal{R}_g$ and $\mathcal{R}_m$; whereas, it may include transmission $\mathcal{R}_t$, final drive $\mathcal{R}_{fd}$, and gear-train $\mathcal{R}_m$ in a parallel HEV. Although power-split HEVs are not investigated in this thesis, its configuration can also be represented by the universal configuration in Fig. 2.11. Assuming the ratio of a planetary gear set is the ratio between radius of ring gear and the one of sun gear, which is $\mathcal{R} = \frac{R_{ring}}{R_{sun}}$, the Toyota Prius Hybrid can be represented by setting corresponding ratios as follows:

$$\mathcal{R}_g = 1 + \mathcal{R}, \tag{2.17}$$

$$\mathcal{R}_t = \frac{\mathcal{R}}{1 + \mathcal{R}}, \tag{2.18}$$

$$\mathcal{R}_e = 1, \tag{2.19}$$

$$\mathcal{R}_m = 1. \tag{2.20}$$

The ratio $\mathcal{R}_{fd}$ is the final drive of the investigated vehicle.

Considering conventional and parallel hybrid-electric vehicles, transmissions specifically refer to multi-gear gearboxes alone in this thesis. In contrast, all the other gear-trains in Fig. 2.11 are considered as simple gear-trains with only one ratio.

Although transmissions can be classified into different types of technologies, the investigated transmissions only include Manual Transmission (MT), Automatic Transmission (AT), and Dual Clutch Transmission (DCT). Thus, the technological parameter of stepped-ratio transmission is

$$\mathcal{I}_t = \{\mathrm{MT}, \mathrm{AT}, \mathrm{DCT}\}, \tag{2.21}$$

which are represented by integers.

2.3.1 Dimensioning Parameter

Except for transmission, the dimensioning parameter set of a drivetrain in generic form is expressed as

$$\mathcal{S}_d = \left\{\mathcal{R}_{fd}, \mathcal{R}_t, \mathcal{R}_m, \mathcal{R}_e, \mathcal{R}_g\right\}. \tag{2.22}$$

As for transmission, the typical dimensioning parameters consist of the ratios of first gear and last gear, and total gear number, which yields

$$\mathcal{S}_t = \{\mathcal{I}_t, \mathcal{R}_{t1}, \mathcal{R}_{tk}, \mathcal{K}_t\}, \tag{2.23}$$

where $\mathcal{R}_{t1}$ and $\mathcal{R}_{tk}$ are gear ratios of the first and last gear, respectively; $\mathcal{K}_t$ is the total gear number.

2.3.2 Analytic Model of Transmissions

Regarding stepped-ratio transmissions, both gear ratios and transmission efficiency are parameterized at descriptive and predictive level below.

At Descriptive Level

The chosen descriptive analytic model of gear ratios for a $\mathcal{K}$-speed transmission ($\mathcal{K} \geq 4$) is

$$\mathcal{R}_t(n_t) = k_{t0} + k_{t1} n_t + k_{t2} n_t^2 + k_{t3} n_t^3 + k_{t4} n_t^4, \tag{2.24}$$

where $\mathcal{R}_t$ represents the gear ratio and n_t is the gear number.

Under the investigation of four-speed transmissions, parameter k_{t4} in Eq. 2.24 is equal to zero; whereas other parameters $k_{ti} (i = 0, 1, \cdots, 3)$ are identified through the

least squares fitting method. This method is implemented as well to identify descriptive parameters for the stepped-ratio transmissions in the identification set of Table 2.7.

In regard to gear efficiency, the chosen descriptive analytic model of the transmission power at the output shaft is modeled by

$$P_{to} = \begin{cases} k_{t5} + k_{t6} P_t, & P_t \geq 0, \\ -k_{t5} + \dfrac{P_t}{k_{t6}}, & P_t < 0, \end{cases} \tag{2.25}$$

where P_t is the transmission power at the input shaft, and P_{to} is the transmission power at output shaft.

At Predictive Level

The specific dimensioning parameters of a stepped-ratio transmission consist of first gear ratio, last gear ratio, and gear number, which are summarized as $\{ \mathcal{R}_{t1}, \mathcal{R}_{tk}, \mathcal{K}_t \}$.

Predictive analytic models of stepped-ratio transmission are developed based on the parameters in the previous descriptive analytic models in Eq. 2.24 and 2.25. Considering predictive analytic models of transmission gear ratio, they are written in the matrix equation form as

$$\begin{bmatrix} k_{t0} \\ k_{t1} \\ \vdots \\ k_{t4} \end{bmatrix} = (\mathcal{R}_{t1} - \mathcal{R}_{tk}) \begin{bmatrix} c_{t1} \\ c_{t2} \\ \vdots \\ c_{t5} \end{bmatrix} + \begin{bmatrix} 1 \\ 0 \\ \vdots \\ 0 \end{bmatrix}, \tag{2.26}$$

where the coefficients $c_{ti} (i = 1, \cdots, 5)$ depend on gear number $\mathcal{K}_t$ and technological parameter $\mathcal{I}_t$. The values are listed in Table 2.6.

$\mathcal{I}_t$	$\mathcal{K}_t$	c_{t1}	c_{t2}	c_{t3}	c_{t4}	c_{t5}
MT	5	2.259	-1.766	0.6009	-0.1	6.485×10^{-3}
DCT	6	2.041	-1.391	0.4023	-0.05578	2.985×10^{-3}
AT	6	1.786	-1.003	0.2473	-0.03035	1.455×10^{-3}

Table 2.6 – Values of coefficients $c_{ti} (i = 1, \cdots, 5)$ for stepped-ratio transmissions.

Note that, the analytic models in Eq. 2.24 and 2.26 are valid solely at the transmission level when the final drive is single-speed. However, in some drivetrain, particularly a dual clutch transmission (DCT), the final drive are typically of two speeds, which are

engaged to specific gears of transmissions. In this case, ratios $\mathcal{R}_{t1}$ and $\mathcal{R}_{tk}$ are considered in terms of the overall gear ratio of transmission and final drive.

In regard to gear efficiency, the predictive analytic models are simplified as in Eq. 2.27 and 2.28 because of limited available transmission efficiency data.

$$k_{t5} = c_{t6}, \tag{2.27}$$

$$k_{t6} = c_{t7}, \tag{2.28}$$

where the coefficient c_{t6} is zero for light-duty transmissions, and -660.6 for heavy-duty transmissions; the coefficient c_{t7} is 0.95 for light-duty transmissions, and 0.977 for heavy-duty transmissions.

2.3.3 Model Validation

The identification set of stepped-ratio transmissions for the light-duty vehicles is presented and used to identify the coefficients in predictive analytic models. After demonstration of results of gear ratios, the relative errors between description of gear ratio and grid-point data and between prediction and grid-point data are comparatively illustrated and discussed in terms of energy consumption of a reference conventional vehicle over different missions.

The verification of efficiency model is carried out only for one transmission in heavy-duty applications. Due to limited available data and the low energy loss, however, the efficiency of stepped-ratio transmissions is assumed to be constant in light-duty applications.

Identification Set

The identification set of stepped-ratio transmissions is composed of five- and six-speed MTs, six-speed ATs, and six-speed DCTs. Main characteristics of these transmissions, including technological parameter $\mathcal{I}_t$, gear number $\mathcal{K}_t$, speed count of final drive $\mathcal{K}_{fd}$, and relating vehicle models, are summarized in Table 2.7. The whole identification set of stepped-ratio transmissions is only for light-duty vehicles.

Result

Description and prediction of each stepped-ratio transmission are comparatively illustrated with respect to the grid-point data. The complete identification set is classified into four groups for the presentation of results, which are five-speed MT (denoted by

ID	$\mathcal{I}_t$	$\mathcal{K}_t$	$\mathcal{K}_{fd}$	Vehicle Model
01	MT	5	1	Suzuki Celerio
02	MT	5	1	Audi A1
03	MT	5	1	BMW 318i
04	MT	5	1	VW Der Polo
05	MT	5	1	Renault CLIO II
06	MT	6	1	Volvo V40
07	MT	6	1	Volvo V40
08	MT	6	1	Audi A3
09	MT	6	1	Audi A5
10	MT	6	1	BMW 116i
11	AT	6	1	Ford Kuga
12	AT	6	1	KIA Sportage
13	DCT	6	2	Ford Kuga
14	DCT	6	2	VW Jetta

Table 2.7 – Identification set of stepped-ratio transmissions.

MT-5), six-speed MT (denoted by MT-6), six-speed AT (denoted by AT–6), and six-speed DCT (denoted by DCT-6).

Results of each group, including grid-point data, description, and prediction, are summarized in Fig. 2.12 with different markers. Markers of dot ($\bullet$), circle ($\circ$), and star ($*$) represent the grid-point data, description, and prediction, respectively. Note that, overall gear ratio is considered in the group of DCTs because that DCTs require duel-speed final drive to constitute the stepped ratios.

Analysis

Analytic models of stepped ratios do not cause any energy losses in Eq. 2.24. However, they affect the operating points of internal combustion engines by shifting engine speed and torque. Therefore, a further analysis was completed to investigate the influences of descriptive and prediction analytic models on the energy consumption of a reference vehicle over two distinct missions. The investigated mission consists of New European Driving Cycle (NEDC) and Highway Fuel Economy Test cycle (HYWFET).

Fig. 2.13 illustrates the results of energy consumption of the reference vehicle with different transmissions from the identification set in Table 2.7. Thanks to descriptive and predictive analytic models in Eq. 2.24 and 2.26, predictions of the energy consumption are close to that evaluated with transmissions of grid-point data over mission profiles of NEDC and HYWFET. The largest error of energy consumption among the investigations

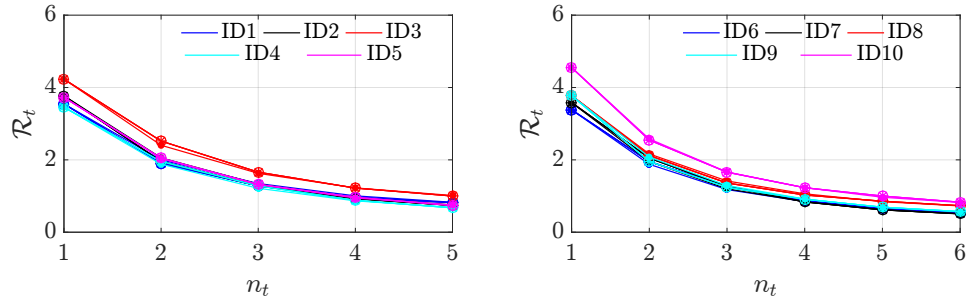

(a) MT-5

(b) MT-6

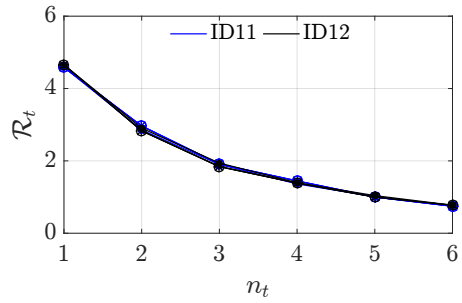

(c) AT–6

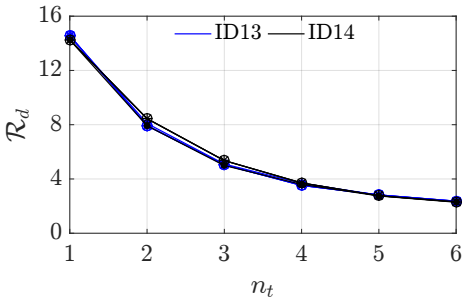

(d) DCT–6

Figure 2.12 – Gear ratio comparison of transmission identification set.

is about 2.7%.

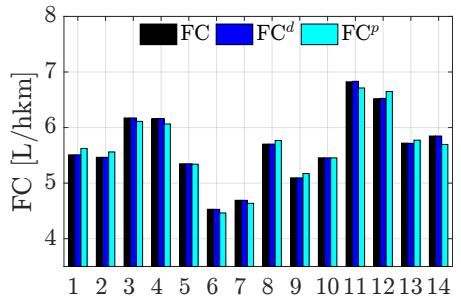

(a) NEDC

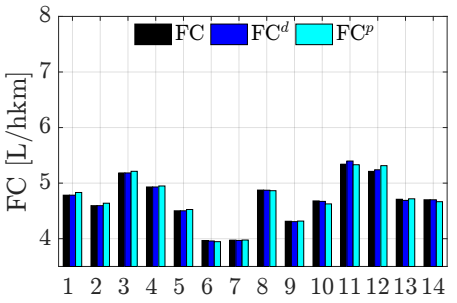

(b) HYWFET

Figure 2.13 – Fuel consumption evaluated with grid-point data, description, and prediction of stepped-ratio transmissions.

Apart from the analysis for analytic models of gear ratios, the analysis for transmission efficiency models is performed in terms of linear regression. The investigated case

is a stepped-ratio transmission for heavy-duty applications.

As shown in Fig. 2.14, results between output power of grid-point data and the one of prediction obtained by Eq. 2.25, 2.27, and 2.28 are presented along the normalized axes. The 5% error lines are depicted with two dashed red lines.

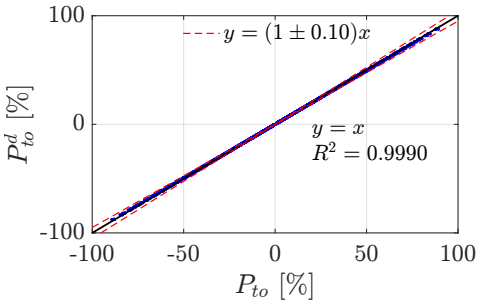

Figure 2.14 – Output power comparison of stepped-ratio transmission.

The the output power of prediction is almost the same as the output power of grid-point data. Yet, the error reduces as the absolute magnitude of the power increase. In other words, the smaller absolute magnitude the power is, the larger the error will be.

2.4 Battery

As an essential electric component in hybrid- and battery-electric vehicles, battery is the energy storage component that releases electric power to propel a vehicle in traction phase, and stores electric energy in the regenerative braking phase. As one of the major technologies in the automotive application, the pouch shape Lithium-Ion Battery (LIB) is classified into two types: High Energy (HE) and High Power (HP) type. These two technological dimensioning parameters of LIB are denoted by $\mathcal{I}_b = \{HE, HP\}$.

2.4.1 Dimensioning Parameter

In an electrified vehicle propulsion system, battery is installed as a battery pack, which contains numerous battery cells in series and/or parallel connection. Battery pack is quantified by battery cell number (denoted by $\mathcal{K}_b$) and nominal parameters of battery cells. Battery cell technology, battery cell number, and battery cell nominal capacity $\mathcal{Q}_b$, are considered as the dimensioning parameters of batteries, which yields

$$\mathcal{S}_b = \{\mathcal{I}_b, \mathcal{K}_b, \mathcal{Q}_b\}. \tag{2.29}$$

2.4.2 Analytic Model

Parameterization of the battery electrochemical and terminal power (denoted by P_{be} and P_b, respectively) is performed for both HE and HP battery cells. The electrochemical and terminal power are calculated based on instantaneous battery state of charge and terminal current. Accordingly, analytic models at both descriptive and predictive level are developed to evaluate the electrochemical power as a function of battery terminal power.

At Descriptive Level

Two different descriptive analytic models are established for specific applications. A piece-wise linear predictive analytic model of battery is tailored for the development of fully analytic energy consumption method for hybrid-electric vehicles, whereas a quadratic predictive analytic model of battery is developed for better accuracy and applied to the rest cases.

The chosen quadratic descriptive analytic model of a battery is written by

$$P_{be}(P_b) = k_{b0} + k_{b1}P_b + k_{b2}P_b^2, \tag{2.30}$$

where parameters $k_{bi}(i = 0, 1, 2)$ are identified for each individual battery in the identification set of battery cells in Table 2.11.

On the other hand, the piece-wise linear descriptive model estimates the electrochemical power with a further limited operating range compared with the one in the battery quadratic mode. The piece-wise linear model is expressed by

$$P_{be}(P_b) = \begin{cases} k_{b3} + k_{b4}P_b, & P_b \geq 0, \\ k_{b5} + k_{b6}P_b, & P_b < 0, \end{cases} \tag{2.31}$$

where parameters $k_{bi}(i = 3, \cdots, 6)$ are identified for each individual battery in the identification set of battery cells in Table 2.11.

At Predictive Level

Corresponding to the descriptive analytic models, two series of predictive models are herein developed. The parameters $k_{bi}(i = 0, \cdots, 6)$ in descriptive analytic models of Eq.

2.30 and 2.31 are further expressed as functions of battery dimensioning parameters.The predictive analytic models for the quadratic descriptive analytic model in Eq. 2.30 are expressed in matrix form as

$$\begin{bmatrix} k_{b0} \\ k_{b1} \\ k_{b2} \end{bmatrix} = \begin{bmatrix} c_{b1} & c_{b2} & c_{b3} \\ c_{b4} & c_{b5} & c_{b6} \\ c_{b7} & c_{b8} & c_{b9} \end{bmatrix} \begin{bmatrix} \mathcal{K}_b \\ \mathcal{Q}_b \\ \frac{\mathcal{Q}_b^2}{\mathcal{K}_b} \end{bmatrix}, \tag{2.32}$$

where coefficients $c_{bi}(i = 1, \cdots, 9)$, depending on the battery technological parameter $\mathcal{I}_b$ and battery cell capacity $\mathcal{Q}_b$, are listed in Table 2.8 and 2.9.

$\mathcal{I}_b$	c_{b1}	c_{b2}	c_{b3}	c_{b4}	c_{b5}	c_{b6}
HP	-9.542	0.5901	-5.868 $\times 10^{-3}$	1.016	-2.219 $\times 10^{-3}$	2.305 $\times 10^{-5}$
HE	0.1	0	0	0.983	-7.617 $\times 10^{-4}$	1.224 $\times 10^{-5}$

Table 2.8 – Values of coefficients $c_{bi}(i = 1, \cdots, 6)$ for lithium-ion battery.

$\mathcal{I}_b$	$\mathcal{Q}_b$	c_{b7}	c_{b8}	c_{b9}
HP	–	1.904×10^{-4}	-2.068×10^{-6}	4.812×10^{-9}
HE	≤ 53 Ah	4.489×10^{-4}	-6.017×10^{-6}	0
	> 53 Ah	1.383×10^{-4}	0	0

Table 2.9 – Values of coefficients $c_{bi}(i = 7, \cdots, 9)$ for lithium-ion battery.

The predictive analytic models for the piece-wise linear descriptive analytic model in Eq. 2.31 are expressed as

$$\begin{bmatrix} k_{b3} \\ k_{b4} \\ k_{b5} \\ k_{b6} \end{bmatrix} = \begin{bmatrix} c_{b10} & 0 & 0 & 0 \\ 0 & c_{b11} & c_{b12} & c_{b13} \\ c_{b14} & 0 & 0 & 0 \\ 0 & c_{b15} & c_{b16} & c_{b17} \end{bmatrix} \begin{bmatrix} \mathcal{K}_b \\ \mathcal{Q}_b \\ \mathcal{Q}_b^2 \\ \mathcal{Q}_b^3 \end{bmatrix}, \tag{2.33}$$

where coefficients $c_{bi}(i = 10, \cdots, 17)$, depending only on the battery technological parameter $\mathcal{I}_b$, are listed in Table 2.10.

2.4.3 Model Validation

The identification set of batteries is introduced and used to identify coefficients in predictive analytic models. After the comparative illustration of battery electrochemical

$\mathcal{I}_b$	c_{b10}	c_{b11}	c_{b12}	c_{b13}
HP	-0.1138	7.741×10^{-2}	-1.745×10^{-3}	1.211×10^{-5}
HE	-0.0628	6.561×10^{-2}	-1.315×10^{-3}	8.368×10^{-6}
$\mathcal{I}_b$	c_{b14}	c_{b15}	c_{b16}	c_{b17}
HP	-0.1767	6.279×10^{-2}	-1.39×10^{-3}	9.548×10^{-6}
HE	-0.1328	6.036×10^{-2}	-1.274×10^{-3}	8.496×10^{-6}

Table 2.10 – Values of coefficients $c_{bi}(i = 10,\cdots,17)$ for lithium-ion battery.

and terminal power of an example, the mean relative error and statistic characteristics are presented and discussed.

Identification Set

The identification set of lithium-ion battery cells, including high energy (HE) and high power (HP) type, is presented in Table 2.11 with technological parameter, nominal voltage, and energy density.

ID	$\mathcal{I}_b$	$\mathcal{Q}_b$ [Ah]	Nominal Voltage [V]	Energy Density [Wh/kg]
1	HE	25	3.7	162
2	HE	31	3.7	166
3	HE	40	3.7	166
4	HE	53	3.7	171
5	HE	75	3.7	178
6	HP	31	3.7	147
7	HP	40	3.7	153
8	HP	63	3.7	156
9	HP	75	3.7	159

Table 2.11 – Identification set of Li-ion battery cells.

Result

For simplicity reason, description and prediction of one exemplified battery cell are comparatively illustrated with respect to the grid-point data. The description and prediction are separately evaluated with the quadratic and piece-wise linear analytic models.

Fig. 2.15 demonstrates the grid-point data, description, and prediction in terms of electrochemical power for BAT ID2. The grid-point data, description, and prediction are

aligned well with each other for both quadratic and piece-wise linear analytic models. However, the maximal charging and discharging current are limited more for the piece-wise linear analytic models. Therefore, the magnitude in Fig. 2.15b is smaller than that in Fig. 2.15a.

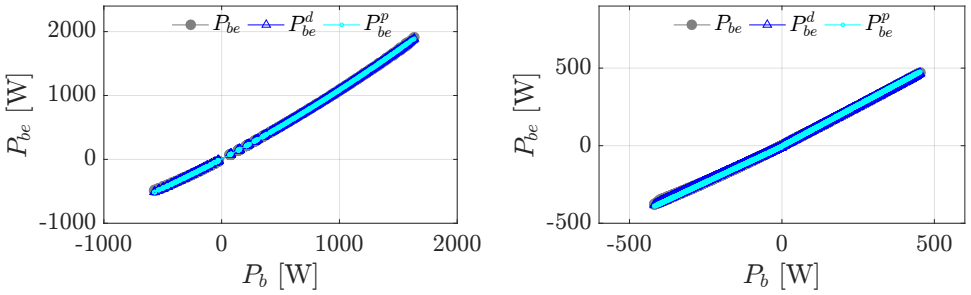

(a) quadratic analytic model (b) piece-wise linear analytic model

Figure 2.15 – Electrochemical power of battery cell ID2.

Analysis

The analysis of mean relative error and linear regression is performed to evaluate the accuracy of descriptive and predictive analytic models for lithium-ion battery cells. In particular, analysis of mean relative error is completed for both battery cells and their whole identifications set. Then, the previous exemplified battery cell is further analysed through linear regression method.

Results of mean relative errors – including the mean description error of each battery cell ε_c^d, the mean prediction error of each battery cell ε_c^p, the average description error of battery cell identification set ε_s^d, and the average prediction error ε_s^p – are illustrated in Fig. 2.16. To summarize, the quadratic analytic model produces less mean relative errors than the piece-wise linear analytic model did at both descriptive and predictive level. Nonetheless, the maximum mean relative error is less than 10% (battery cell ID4) which is evaluated via the piece-wise linear analytic model.

Considering the linear regression analysis for battery cell ID2, results are summarized in Fig. 2.17. Both description and prediction of different types of analytic models are separately compared with respect to the grid-point data. Obviously, high relative errors occurs at the low absolute power region.

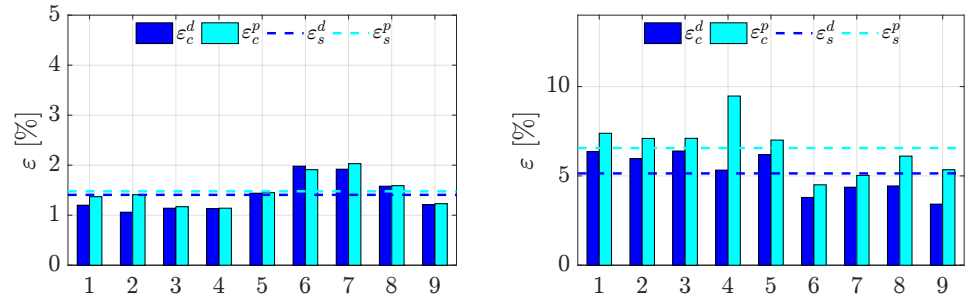

(a) quadratic model (b) piece-wise linear model

Figure 2.16 – Mean relative errors of battery identification set.

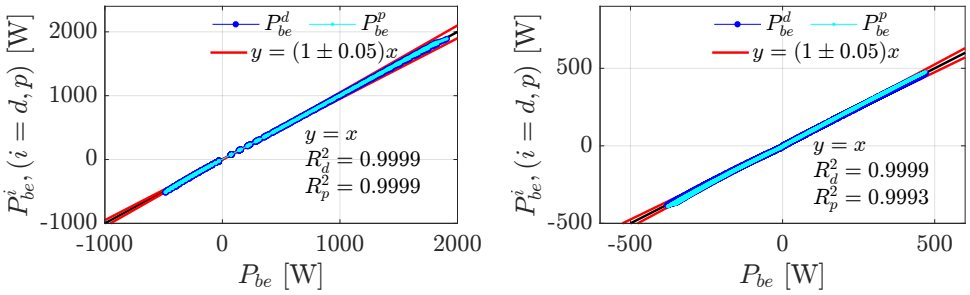

(a) quadratic analytic model (b) piece-wise linear analytic model

Figure 2.17 – Comparison of electrochemical power of battery for battery cell ID2.

2.5 Electric Motor/Generator

Electric Motor/Generator (EMG) is another essential component in an electrified vehicle propulsion system to convert the energy form, such as from electric power to mechanical one, or vice versa. Two types of EMGs are frequently applied in the automotive applications, which are the Permanent Magnet Synchronous Machine (PMSM) and the Asynchronous Induction Machine (AIM). Therefore, the technological parameter of EMG consists of $\mathcal{I}_m = \{\text{PMSM}, \text{AIM}\}$.

2.5.1 Dimensioning Parameter

An EMG is dimensioned by its nominal torque and power, maximal torque and power, maximum rotational speed in vehicle propulsion systems. In order to evaluate energy consumptions of hybrid- and battery-electric vehicles, the dimensioning parameters are

simplified as nominal torque and nominal power. Meanwhile, peak torque and peak power are assumed to be identical to the nominal torque and power, respectively.

Because the nominal power is the product of the motor base speed and the nominal torque, the dimensioning parameter of nominal power is substituted by the base speed. Thus, the dimensioning parameter set of electric motor/generators is expressed as

$$\mathcal{S}_m = \{\mathcal{I}_m, \mathcal{T}_m, \mathcal{N}_m\}, \tag{2.34}$$

where $\mathcal{T}_m$ is the nominal torque, and $\mathcal{N}_m$ is the base speed. Note that, subscript m refers to electric motor; whereas subscript g represents electric generator.

2.5.2 Analytic Model

Parameterization of the energy maps is performed to both types of EMGs. Accordingly, analytic models at both descriptive and predictive level are separately developed and validated. Both the losses of an electric machine and the one of power electronics are lumped into the energy map to identify.

At Descriptive Level

Regardless of technologies of electric motor/generators, the chosen descriptive analytic model is always expressed by

$$P_{me}(\omega_m, P_m) = k_{m0} + k_{m1}\omega_m + k_{m2}\omega_m^2 + k_{m3}P_m + \frac{k_{m4}}{\omega_m^2}P_m^2, \tag{2.35}$$

where ω_m is the rotational speed in [rad/s], P_m is the mechanical power in [W], and P_{me} is the electric power in [W]. Parameters $k_{mi}(i = 0, \cdots, 4)$ are identified for each individual electric motor/generator in Table 2.14 and 2.15.

At Predictive Level

The parameters $k_{mi}(i = 0, \cdots, 4)$ in the descriptive analytic model of Eq. 2.35 are further expressed as functions of the dimensioning parameters of electric motor/generators.

These predictive analytic models are expressed in matrix form, such as

$$\begin{bmatrix} k_{m0} \\ k_{m1} \\ k_{m2} \\ k_{m3} \\ k_{m4} \end{bmatrix} = \begin{bmatrix} c_{m1} & c_{m2} & c_{m3} & c_{m4} & c_{m5} & c_{m6} \\ c_{m7} & c_{m8} & c_{m9} & c_{m10} & c_{m11} & c_{m12} \\ c_{m13} & c_{m14} & c_{m15} & c_{m16} & c_{m17} & c_{m18} \\ c_{m19} & 0 & 0 & 0 & 0 & 0 \\ c_{m20} & c_{m21} & c_{m22} & c_{m23} & c_{m24} & c_{m25} \end{bmatrix} \begin{bmatrix} 1 \\ \mathcal{T}_m \\ \mathcal{T}_m^2 \\ \frac{\pi \mathcal{N}_m}{30} \\ \frac{\pi^2 \mathcal{N}_m^2}{30^2} \\ \frac{\pi \mathcal{N}_m \mathcal{T}_m}{30 \times 10^3} \end{bmatrix}, \tag{2.36}$$

where coefficients $c_{mi}(i = 1, \cdots, 25)$, depending on the technological parameter $\mathcal{I}_m$, are listed in Table 2.12 and 2.13; whereas coefficient c_{m19} is 1 for both PMSM and AIM.

$\mathcal{I}_m$	c_{m1}	c_{m2}	c_{m3}	c_{m4}	c_{m5}	c_{m6}
PMSM	270.7	-13.738	0.0714	0.228	-3.681×10^{-4}	8.782
IM	5665.7	-30.811	0.0332	-3.759	-2.618×10^{-3}	25.331
$\mathcal{I}_m$	c_{m7}	c_{m8}	c_{m9}	c_{m10}	c_{m11}	c_{m12}
PMSM	-1.215	0.0608	-2.778×10^{-4}	-4.775×10^{-4}	1.331×10^{-6}	-0.0374
IM	-0.326	0.0222	-2.621×10^{-5}	-7.089×10^{-3}	8.615×10^{-6}	1.859×10^{-5}
$\mathcal{I}_m$	c_{m13}	c_{m14}	c_{m15}	c_{m16}	c_{m17}	c_{m18}
PMSM	2.333×10^{-3}	-7.110×10^{-6}	7.062×10^{-8}	-3.476×10^{-6}	1.480×10^{-9}	2.650×10^{-5}
IM	-1.224×10^{-3}	7.484×10^{-6}	-1.114×10^{-10}	5.998×10^{-6}	-4.239×10^{-9}	-1.118×10^{-5}

Table 2.12 – Values of coefficients $c_{mi}(i = 1, \cdots, 18)$ for electric motor/generator.

$\mathcal{I}_m$	c_{m20}	c_{m21}	c_{m22}	c_{m23}	c_{m24}	c_{m25}
PMSM	0.4441	-0.01356	7.245×10^{-5}	0.001948	2.9231×10^{-7}	-6.7541×10^{-3}
IM	1.044×10^{-3}	5.846×10^{-5}	-3.703×10^{-7}	4.650×10^{-4}	-2.359×10^{-7}	-8.128×10^{-5}

Table 2.13 – Values of coefficients $c_{mi}(i = 20, \cdots, 25)$ for electric motor/generator.

2.5.3 Model Validation

The identification sets of EMGs, generated by EMTool [66], are presented at the beginning in terms of PMSMs and AIMs, respectively. After the demonstration of electric motor grid-point data in terms of contour maps, the mean relative error and statistic characteristics are summarized and discussed.

Identification Set

Due to different vehicle applications, two types of identification sets are used to develop and validate the descriptive and predictive analytic models. The identification set of permanent magnet synchronous machine is listed in Table 2.14, including specifications of dimensioning parameters; whereas the identification set of induction machines is summarized in Table 2.15.

Note that, the maximum speed of PMSM and AIM identification set is 20 and 14 krpm, respectively. These values are close to the FLEX HEV developed by IFPEN and early generation of Tesla's electric motor.

ID		1	2	3	4	5	6	7	8
$\mathcal{T}_m$	[Nm]	36	36	36	36	36	72	72	72
$\mathcal{P}_m$	[kW]	15	21	26	32	38	30	41	53
ID		9	10	11	12	13	14	15	
$\mathcal{T}_m$	[Nm]	72	72	108	108	108	108	108	
$\mathcal{P}_m$	[kW]	64	75	45	62	79	96	113	

Table 2.14 – Identification set of electric motor/generators in terms of PMSM.

ID		1	2	3	4	5	6	7	8
$\mathcal{T}_m$	[Nm]	270	270	270	270	330	330	330	330
$\mathcal{P}_m$	[kW]	85	113	141	170	104	138	173	207
ID		9	10	11	12	13	14	15	16
$\mathcal{T}_m$	[Nm]	390	390	390	390	450	450	450	450
$\mathcal{P}_m$	[kW]	123	163	204	245	141	188	136	238

Table 2.15 – Identification set of electric motor/generators in terms of AIM.

Result

Description and prediction of each electric motor/generator are comparatively illustrated with respect to the grid-point data. For the sake of simplicity, one PMSM and one AIM are depicted and discussed separately. The comparison among grid-point data, description, and prediction of other electric motor/generators are found in Appendix B.2.

Fig. 2.18 demonstrates the grid-point data, description, and prediction in terms of terminal electric power of PMSM ID14, whereas Fig. 2.19 illustrates the grid-point data,

description, and prediction of AIM ID14. The high efficiency zones are enlarged with the description and the prediction compared with the grid-point data for both electric machines. Nonetheless, both description and prediction are still close to the grid-point data. In addition, AIMs work better with the developed analytic models than PMSMs do.

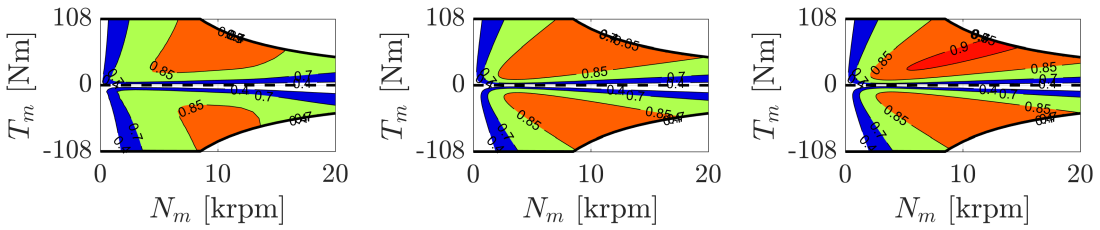

(a) grid-point data (b) description (c) prediction

Figure 2.18 – Efficiency map of PMSM ID14.

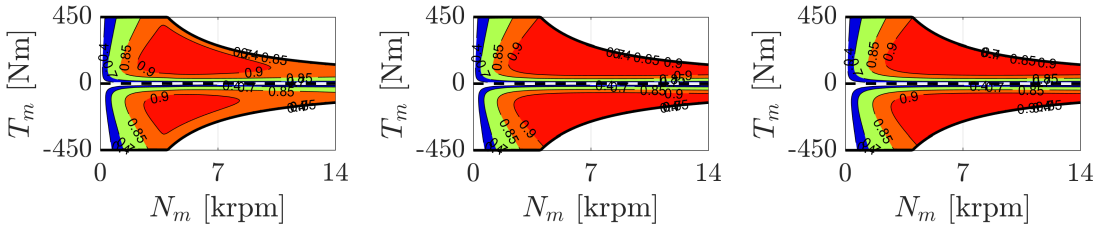

(a) grid-point data (b) description (c) prediction

Figure 2.19 – Efficiency map of AIM ID14.

Analysis

The analysis of mean relative error and linear regression are performed to evaluate the accuracy of descriptive and predictive analytic models for both PMSMs and AIMs. In particular, analysis of mean relative error is completed both for each electric machine and the whole identifications set. Then, the exemplary electric machines depict their contour maps of mean relative error and perform the linear regression analysis.

Mean relative errors – including the mean description error of each component ε_c^d, the mean prediction error of each component ε_c^p, the average description error of whole identification set ε_s^d, and the average prediction error of whole identification set ε_s^p – are illustrated in Fig. 2.20 for both PMSMs and AIMs. In summary, the maximum of mean relative error is slightly higher than 10% for AIM ID6. The mean relative error of the identification set of PMSM is lower than that of AIMs.

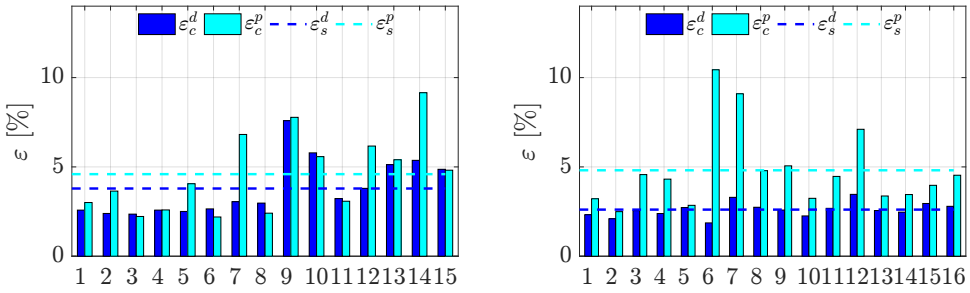

(a) PMSM (b) AIM

Figure 2.20 – Mean relative error of each electric motor/generator and the whole identification set.

Considering PMSM ID14, its descriptive and predictive relative errors are illustrated in Fig. 2.21a and 2.21b, respectively. The high errors occur at the low torque area. The error in the low-speed high-torque in the generator mode is the intrinsic error from the estimation of EMTool.

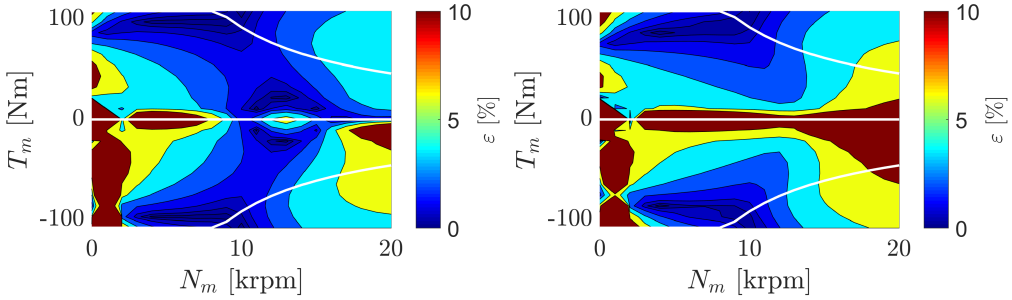

(a) description error map (b) prediction error map

Figure 2.21 – Maps of relative errors of PMSM ID14.

As for AIM ID14, its descriptive and predictive relative errors are illustrated in Fig. 2.22a and 2.22b, separately. Compared with previous case, AIM ID14 shows larger low efficiency area in description and prediction error map, respectively. Yet, the intrinsic error of EMTool is still presented in the low-speed high-torque zone in the generator mode.

Regarding the linear regression analysis, Fig. 2.23 and 2.24 compare the results of electrical power of PMSM ID14 and AIM ID14, respectively. The relative error of the description is limited within 10%, whereas most of relative error of the prediction is limited within 10%.

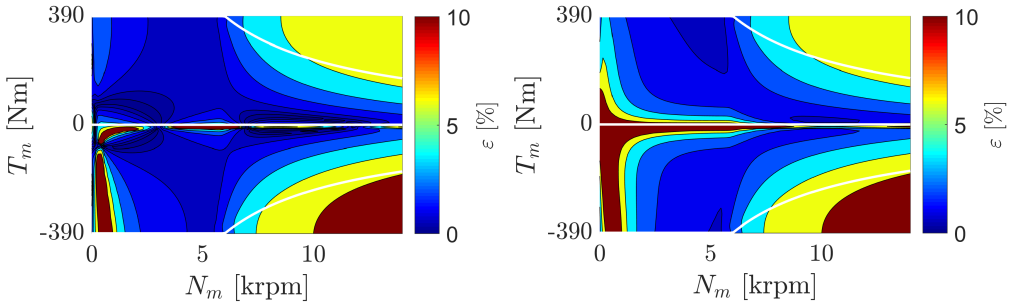

(a) description (b) prediction

Figure 2.22 – Maps of relative errors of AIM ID14.

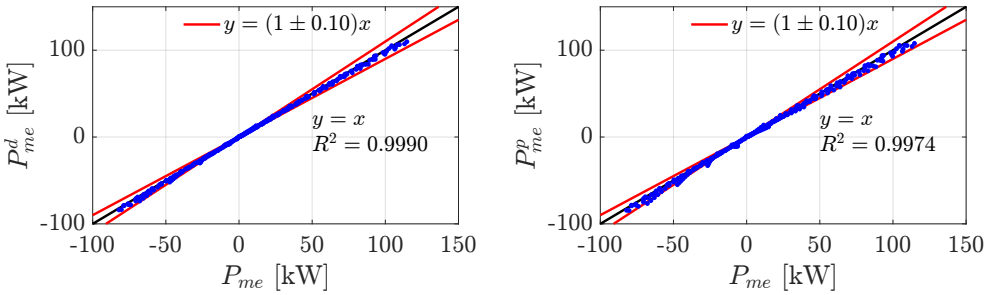

(a) description (b) prediction

Figure 2.23 – Comparison of electric power of PMSM ID14.

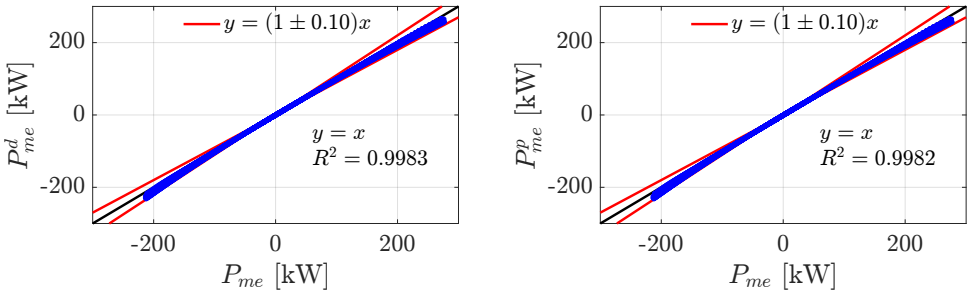

(a) description (b) prediction

Figure 2.24 – Comparison of electric power of AIM ID14.

2.6 Vehicle Load Estimation

Apart from the dimensioning parameters of main powertrain components, vehicle parameters affect the energy consumption as well because of the impacts on vehicle load. In analogue to powertrain dimensioning parameter set, the vehicle parameter set is defined as

$$\mathcal{S}_v = \{m_v, R_w, C_{v0}, C_{v1}, C_{v2}\}, \tag{2.37}$$

where m_v is the weight of vehicle in [kg], R_w is the wheel radius in [m], $C_{vi}(i = 0, 1, 2)$ are load parameters identified through coast-down tests.

The vehicle longitudinal dynamics is the essence in vehicle load estimation for the energy consumption evaluation. Considering a vehicle moving on an inclined road as depicted in Fig. 2.25, the vehicle load is evaluated by

$$F_l = C_{v0}\cos\alpha + C_{v1}v\cos\alpha + C_{v2}v^2 + F_{gr} + F_{ir}, \tag{2.38}$$

where F_{gr} is the gravitational force calculated by $F_{gr} = m_v g \sin\alpha$, and F_{ir} is the inertia force due to acceleration and deceleration.

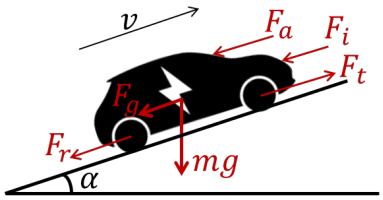

Figure 2.25 – Longitudinal forces acting on a vehicle moving on an inclined road.

Considering the road load parameters $C_{vi}(i = 0, 1, 2)$, they can be approximated with physical ones by

$$C_{v0} \approx m_v g C_{rr}, \tag{2.39}$$

$$C_{v1} \approx 0, \tag{2.40}$$

$$C_{v2} \approx \frac{\rho_{ar} C_{ar} A_{ar}}{2}, \tag{2.41}$$

where C_{rr} is rolling resistance coefficient, C_{ar} is drag coefficient, A_{ar} is frontal area, and ρ_{ar} is air density.

As for the vehicle mass m_v, it depends on the dimensioning parameters of powertrain components, which yields

$$m_v = m_{v0} + \mu_e \mathcal{V}_e + \mu_b \mathcal{E}_b + \mu_m \mathcal{P}_m + \mu_g \mathcal{P}_g, \tag{2.42}$$

where $\mu_i (i = e, b, m, g)$ is a generic weight factor in kilogram per unit, and m_{v0} is the baseline weight of vehicle.